nature communications

Article

https://doi.org/10.1038/s41467-025-56649-5

Lattice-driven gating in a Cu-based zeolitic imidazolate framework for efficient high-temperature hydrogen isotope separation

Received: 11 July 2024

Accepted: 22 January 2025

Published online: 27 February 2025

Check for updates

Minji Jung[1,8], Jaewoo Park[1,8], Raeesh Muhammad[1,8], Taeung Park[2], Sung-Yeop Jung[1], Jungwon Yi[1], Cheolwon Jung[3], Jacques Ollivier[4], Anibal J. Ramirez-Cuesta[5], Jitae T. Park[6], Jaheon Kim[3] ✉, Margarita Russina[7] ✉ & Hyunchul Oh[1,2] ✉

For the separation of hydrogen isotopes (H_2/D_2), traditional kinetic quantum sieving (KQS) takes advantage of the diffusion barriers created by the flexibility of organic linkers and the breathing frameworks in porous solids. While the phenomena have been observed typically below 77 K, in this study, we present that a copper-based zeolite imidazolate framework (Cu-ZIF-gis) can show KQS above 120 K. Since Cu-ZIF-gis has narrow channels with ca. 2.4 Å in aperture, the small pore size itself acts as a diffusion barrier. This barrier changes with temperatures, leading to pore contraction or expansion through lattice-driven gating (LDG). The H_2 adsorption isotherms measured at 40 – 150 K reflect the temperature sensitivity of the pore properties. Quasi-elastic neutron scattering (QENS) experiments indicate a notable difference in the molecular mobility of H_2 and D_2, even at temperatures exceeding 150 K. Temperature-variation powder X-ray diffraction measurements at 20 – 300 K show a small but gradual increase in the unit cell volume, indicating that LDG gives rise to the KQS at temperatures above 120 K. These findings can be applied to develop sustainable isotope separation technologies using existing LNG cryogenic infrastructure.

Deuterium, a stable isotope of hydrogen, plays a critical role in enhancing the durability and luminous efficiency of semiconductors and display devices, as well as serving as a fusion fuel for energy production[1,2]. By exchanging hydrogen-deuterium at the interface, for instance, semiconductor devices can improve their lifespan by 10–50 times[3]. This significant improvement has garnered considerable interest from the electronics industry. Consequently, there is a growing demand for energy-efficient and environmentally sustainable hydrogen isotope separation technologies. However, separating hydrogen isotopes in industrial processes poses significant challenges due to their identical physicochemical properties, leading to energy-intensive operations and low selectivity at elevated temperatures[4]. Traditional methods like cryogenic distillation dominate the field but are notorious for their high energy consumption and operational inefficiencies[5]. Although effective at low temperatures, these techniques struggle

[1]Department of Chemistry, Ulsan National Institute of Science and Technology (UNIST), Ulsan, Republic of Korea. [2]Graduate School of Carbon Neutrality, Ulsan National Institute of Science and Technology (UNIST), Ulsan, Republic of Korea. [3]Department of Chemistry, Soongsil University, Seoul, Republic of Korea. [4]Institute Laue-Langevin, 71 avenue des Martyrs CS 20156, 38042, Grenboble, Cedex, France. [5]Neutron Scattering Division, Oak Ridge National Laboratory, Oak Ridge, Tennessee, USA. [6]Heinz Maier-Leibnitz Zentrum (MLZ), Technische Universität München, Garching, Germany. [7]Helmholtz Zentrum Berlin fur Materialien und Energie Hahn-Meitner-Platz 1, Berlin, Germany. [8]These authors contributed equally: Minji Jung, Jaewoo Park, Raeesh Muhammad. ✉e-mail: jaheon@ssu.ac.kr; margarita.russina@helmholtz-berlin.de; hcoh@unist.ac.kr

to maintain performance as temperatures rise, leading to increased costs and environmental impacts.

Recently, confined porous systems have emerged as efficient methods for hydrogen isotope separation. For example, metal-organic frameworks (MOFs) can separate isotopes through nuclear quantum effects, which amplify the isotope effect due to the large mass ratio between H_2 and D_2[6]. Two primary nuclear quantum effects, Kinetic Quantum Sieving (KQS) and Chemical Affinity Quantum Sieving (CAQS), have been explored for D_2/H_2 separation. CAQS depends on the differences in zero-point energy (ZPE) of hydrogen isotopes. D_2 exhibits a lower ZPE and, as a result, has a stronger binding energy, which improves separation efficiency[7–14]. While CAQS-based isotope separation demonstrates high selectivity at elevated temperatures and appears promising[8,13,15–18], it requires strong adsorption sites, raising concerns about the structural durability of the adsorbents[19]. In contrast, KQS leverages the difference in de Broglie wavelengths of the isotope molecules at cryogenic temperatures. Therefore, employing a structurally stable method like KQS for hydrogen isotope separation at high temperatures would be advantageous for practical applications.

To achieve efficient KQS, it is essential to create differences in diffusion barriers for selected isotopes. Current representative KQS methods utilize two main phenomena in MOFs: *the breathing phenomenon*, where the entire framework structure undergoes rapid changes, and *local flexibility*, where certain molecules or atoms at the aperture vibrate. Both phenomena, which facilitate isotope separation, are generally observed at temperatures below 77 K. The selectivity for hydrogen isotopes ($S_{D2/H2}$) during KQS decreases with increasing temperature as these barrier differences typically vanish above 77 K. For example, in the breathing phenomenon, Kim et al. observed a decline in $S_{D2/H2}$ in MIL-53(Al) from 13.6 at 40 K/10 mbar to 2.05 at 70 K/10 mbar[20]. Similarly, in the case of local flexibility, Teufel et al. and Muhammad et al. reported reductions in $S_{D2/H2}$ from 6.9 at 40 K to 2.8 at 70 K in MFU-4(Zn) and from 16.7 at 25 K to 2.9 at 60 K in CoFA, respectively, as temperatures increased[9,21].

We have noticed that *thermal gating* can be another approach to achieving high selectivity for KQS at elevated temperatures in a relatively rigid structure. Temperature-dependent pore size modulation in MOFs can dynamically control effective pore sizes to optimize gas separation[22–24], where selective gas adsorption is facilitated based on temperature changes; this approach has been effective for various gas storage and separation applications, including CO_2[25], CH_4[26], H_2[27], and N_2[28]. *Thermal gating* can also apply to H_2/D_2 separation. For instance, a covalent organic framework (COF) functionalized with pyridine shows thermal pore opening with the maximum uptake at 50 K and demonstrated the $S_{D2/H2}$ of 3.8 at 50 K and 14 mbar[14]. FMOF-Cu possesses three interconnected cavities with bottleneck apertures measuring 3.6 Å and 2.5 Å, and all cavities are fully accessible at 77 K with a maximum $S_{D2/H2}$ of 4 at 77 K and 50 mbar[29]. Recently, a metal-organic cage (MOC), 2α, also recorded the maximum uptake at 77 K, and its $S_{D2/H2}$ of 2.8 was recorded at 77 K/200 mbar[30]. These examples aim to make locally flexible dangling molecules or atoms more rigid so that vibrations would only occur at high temperatures, which is interesting but has not yet been accomplished for H_2/D_2 separation above 100 K thus far.

Hence, we propose a strategy called the *Lattice-driven Gating (LDG)* effect, a particular type of *thermal gating*, based on the hydrogen isotope adsorption/desorption and H_2/D_2 separation experiments conducted with Cu-ZIF-gis. Cu-ZIF-gis is a Cu-based zeolitic imidazolate framework, which is a subclass material of MOFs. *Lattice-driven gating* uses the expansion of the entire lattice to modulate the pore size at higher temperatures than 100 K. The H_2 binding energetics of Cu-ZIF-*gis* is significant as the complete desorption requires heating up to ~ 200 K, the highest H_2 desorption temperature range for any MOFs without open metal sites. Thus, Cu-ZIF-*gis* has the potential to show high $S_{D2/H2}$ through KQS. Unlike previous studies that required low operational temperatures, our findings demonstrate the potential of Cu-ZIF-*gis* to integrate seamlessly into existing infrastructures, such as those used in LNG (at 111 K) processing.

Results

Pore structure characterization and single-gas sorption isotherm of Cu-ZIF-*gis*

Cu-ZIF-*gis* was synthesized according to the previous literature method, a solvothermal reaction between $Cu(NO_3)_2{\cdot}3H_2O$ and 2-nitroimidazole (nImH) in *N,N*-dimethylformamide (DMF) (see experimental section)[31]. The powder X-ray Diffraction (XRD), FT-IR, and thermal gravimetric analysis (TGA) data of Cu-ZIF-*gis* matched well with the previous report (Fig. 1a, b and Supplementary Figs 1, 2)[31]. Cu-ZIF-*gis* is a stable material in air for almost three years, which is a beneficial property for practical application (Fig. 1b). The structure consists of 2-nitroimidazolate (nIm) linkers and tetrahedral copper(II) nodes, resulting in the gis-type three-dimensional framework. Due to the highly-flattened tetrahedral Cu(II) centers, the three-dimensional gis framework is squeezed along the crystallographic *c*-axis, giving a much denser and more rigid structure than the uncompressed Zn-ZIF-6-gis[31]. There are three types of pores along the crystallographic *c*-axis: (A) cylindrical straight channels with a cross-sectional diameter of 2.32 ~ 2.44 Å, (B) slanted cylindrical pores connected through small windows and (C) trigonal cylinders with also connected very narrow windows. The nIm linkers along the c-axis almost isolate them. Since the openings of channels B and C are nearly closed by the nIm linkers, only straight channel A is practically usable for gas adsorption. Considering the kinetic diameter of H_2 (2.89 Å) and the incorporated nIm linkers, Cu-ZIF-*gis* may exhibit a structural deformation akin to stimuli-responsive ZIFs[32]. As expected, nitrogen cannot enter at 77 K due to the large kinetic diameter of N_2 (3.64 Å) (Supplementary Fig. 3)[31]. In contrast, O_2 with a kinetic diameter of 3.47 Å could be adsorbed in Cu-ZIF-gis based on the isotherms measured at 90–210 K. The isotherms showed a maximum uptake at 135 K with large hysteresis, after which the hysteresis became weak and disappeared as temperature increased further (Fig. 1c and Supplementary Fig. 4). Since the O_2 kinetic diameter is significantly larger than the pore aperture, this unexpected result can be understood only when pores expand as temperature changes. Similarly to O_2, H_2 diffused inside at 77 K with a large sorption hysteresis (Supplementary Fig. 3). Both the hysteretic and complicated H_2 adsorption behavior may be ascribed to the temperature-dependent, adsorption-induced structural response of the Cu-ZIF-gis as previously reported[31] (Supplementary Figs. 5–7 and Supplementary Table S1). These observations suggest that the Cu-ZIF-gis will efficiently separate D_2/H_2 when the pore size becomes optimal for KQS at a specific temperature range, which should be verified in this work.

The measured H_2 and D_2 adsorption isotherms of Cu-ZIF-gis at 40 K to 150 K give the possibility of allowing H_2/D_2 separation (Fig. 2a, b). The maximum uptake amount is 1.7 mmol g^{-1} for H_2 and 2.3 mmol g^{-1} for D_2 at 100 K, respectively, and the D_2 uptake is higher than H_2 in all the measured isotherms. This difference in adsorption affinities of the hydrogen isotopes is attributed to the quantum confinement effect in Cu-ZIF-gis[33]. Another notable point is the large hysteresis in the isotherms at the temperature range. Even at 120 K, the hysteresis loop is still observable respectively for H_2 and D_2. Since adsorption equilibrium is not achieved under measurable conditions, there should be a substantial diffusion limitation for H_2 and D_2 in the pores, which is the basis of KQS.

The H_2 and D_2 adsorption isotherms at 40–150 K give an assumption for the adsorption processes, proposed as LDG. The progress of the maximum gas uptake at 40–100 K is the reverse of those of common porous materials whose adsorption capacity decreases in proportion to temperature increase. The more considerable gas uptake at higher temperatures is a typical sign of *thermal gating*; the pores become more accessible with increasing sorption temperature

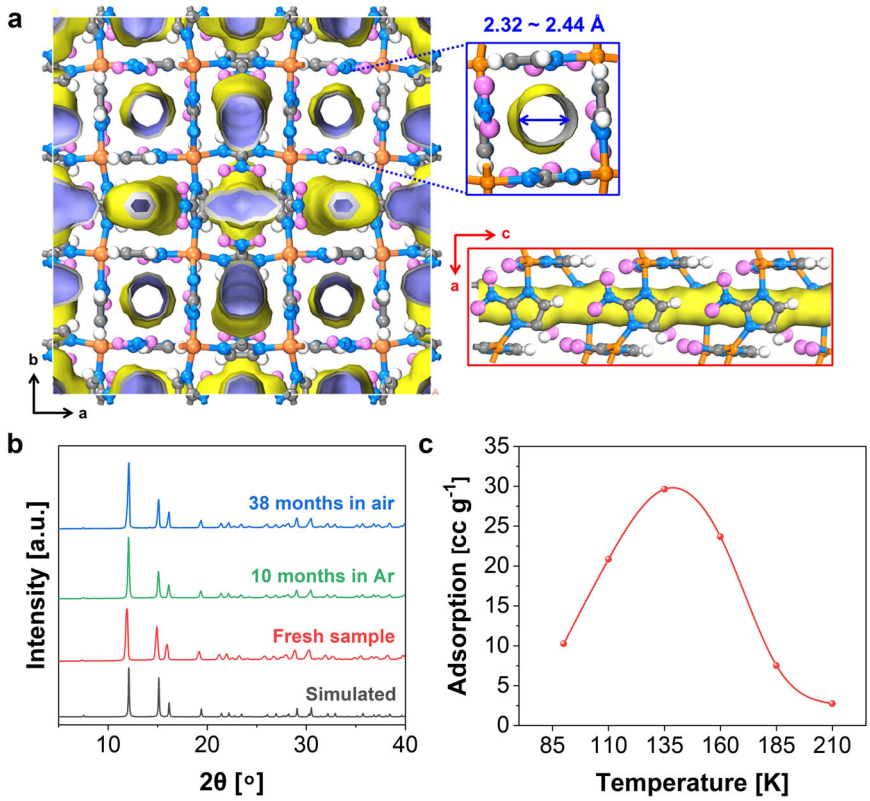

Fig. 1 | Framework characteristics and temperature-dependent sorption of Cu-ZIF-*gis*. **a** The crystal structure of Cu-ZIF-*gis* that shows cylindrical straight channels along the *c*-axis[31]. The pores were calculated with Connolly surfaces with a probe of 1.1 Å. (Cu, orange; N, blue; C, gray; O, magenta; H, white). **b** The powder XRD patterns of the samples after prolonged exposure to Ar and air are compared with that of the as-synthesized fresh sample. **c** The maximum uptake of O_2 measured at various temperatures (90–210 K) in Cu-ZIF-*gis*.

and can accommodate more gas molecules up to 100 K. In Cu-ZIF-gis, the pores are the channels along the *c*-axis, where the ZIF four-membered rings (4MRs) act as channel walls and simultaneously define the entrances to the inner space of all the channels. Therefore, the diffusion of hydrogen molecules can be enhanced only when the entire framework or the lattice expands concertedly to widen the 4MRs. In this regard, *lattice-driven gating* in this work is discerned from known *thermal gating*. In addition, since the cross-section of the 4MRs cannot dramatically expand as temperature increases, the hydrogen isotopes do not diffuse in the pores freely up to 120 K, giving rise to slow equilibrium and hysteresis.

Temperature-varied XRD measurements support how Cu-ZIF-gis responds to a temperature change in terms of *lattice-driven gating*. The XRD peaks corresponding to the (4 0 0), (3 0 1), and (4 1 1) planes at 2θ = 15.1, 16.2, and 19.4°, respectively, were recorded from 20 K to 300 K by heating a sample at 3 K min^{-1} under a high vacuum (Fig. 2c). We could observe the peak shift to lower diffraction angles, indicative of lattice expansion. In more detail, all the data points were converted to the lattice parameters, *a* and *c*, and the unit cell volume and plotted against temperatures (Supplementary Fig. S8). As temperature increases, the unit cell volume increases with a more prominent expansion of the *a*-axis over the *c*-axis. The size of the 4MRs is directly related to the *a*-axis length in a tetragonal unit cell, and conversely, the *a*-axis expansion should lead to the expansion of the cross-sections of the whole channels. Indeed, this temperature-responsive *lattice-driven gating* has not been observed in the known rigid MOFs and ZIFs, which do not show apparent peak shifts in their XRD patterns under temperature variation[34–36].

Hydrogen isotope separation performance

The temperature-responsive *lattice-driven gating* makes the pores accessible to isotopes at ambient temperature, which can be supported by Advanced Cryogenic Thermal Desorption Spectroscopy (AC-TDS) measurements. This analysis of Cu-ZIF-gis gives information on the desorption behavior and separation performance of hydrogen isotopes. The TDS spectra of single-component H_2 and D_2 were measured at their respective liquefaction temperature (20 K for H_2 and 23 K for D_2) and room temperature, respectively (Supplementary Figs. 9, 10). Similar to single-component H_2 and D_2 isotherm studies, no desorption signal was observed when gas was dosed at 20 K or 23 K, while the clear desorption curves starting from 80 K to 190 K were observed after loading at room temperature for both H_2 and D_2, with calculated amounts of 1.7 mmol g^{-1} and 2.2 mmol g^{-1}, respectively. The desorption signal for pure isotope exposure at the liquefaction temperature was not observed because the structure of Cu-ZIF-*gis* was in a closed gate state, blocking hydrogen isotopes from entering the pore. When hydrogen isotopes are exposed to Cu-ZIF-*gis* at room temperature and then cooled to 18 K, the structure locks into a closed gate state after adsorbing the isotopes. This observation means that any isotopes already inside the Cu-ZIF-*gis* from the room-temperature exposure are trapped inside. By that, desorption of trapped isotopes requires high thermal energy, extending up to 180 K for complete release. Notably, the desorption peak maxima of *ca*. 130 K is one of the highest desorption temperatures among MOFs without strong binding sites (open metal sites) reported so far. As a result, the temperature-dependent LDG effect makes the pores accessible to isotopes at high temperatures.

Pure H_2 and D_2 TDS patterns of Cu-ZIF-*gis* were compared with various porous materials to gain insights into the desorption behavior of hydrogen isotope at high temperatures, as shown in Fig. 3a. Six representative samples are compared regarding the desorption curve, which is correlating sorption enthalpy and pore size. MOF-303, with an aperture size of 6 Å, exhibits a TDS spectrum that undergoes complete

https://doi.org/10.1038/s41467-025-56649-5

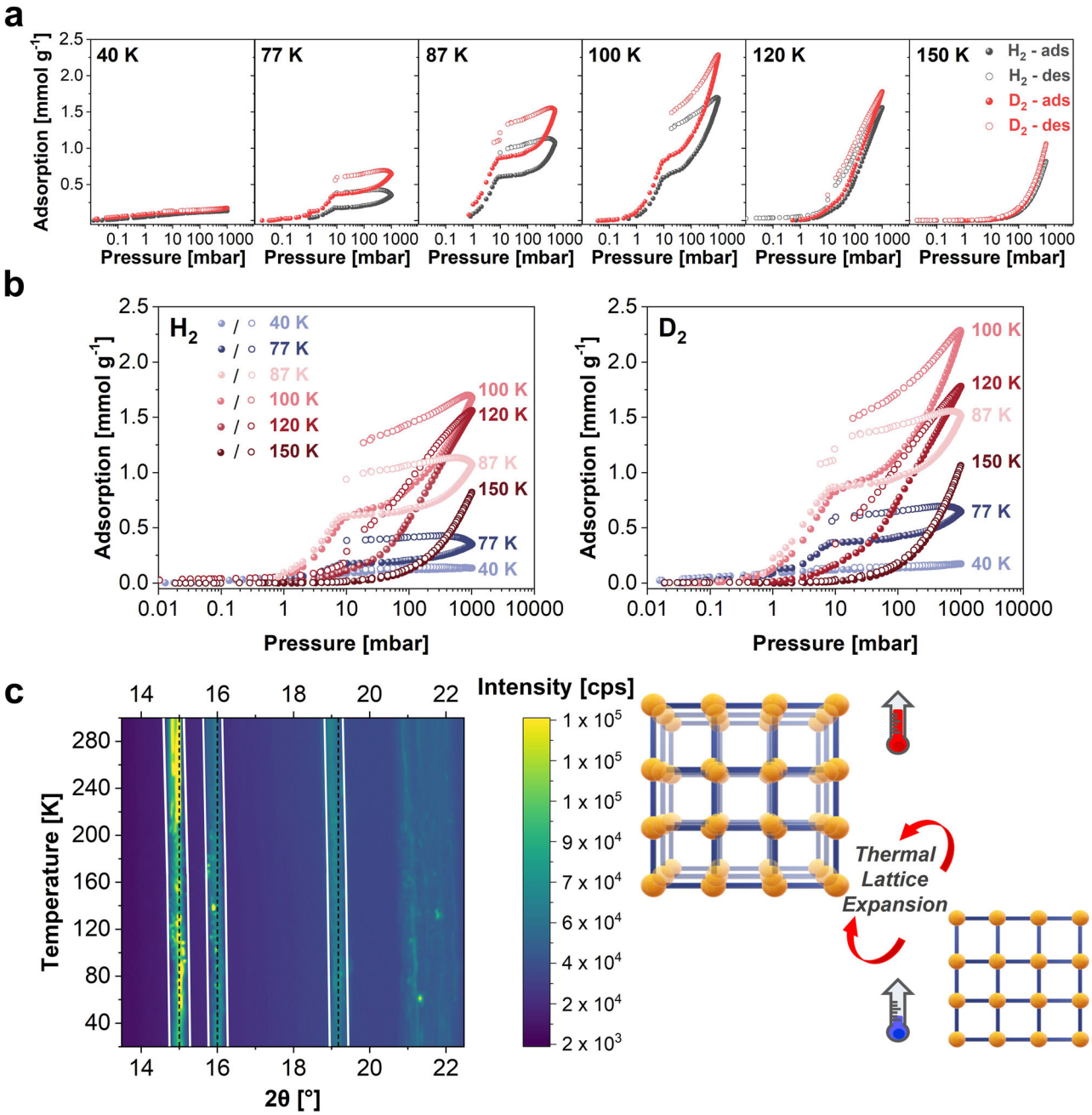

Fig. 2 | Hydrogen isotope adsorption performance at various temperatures and gate opening of Cu-ZIF-*gis*. a The comparison of sorption isotherms for H_2 (black) and D_2 (red) at various temperatures in Cu-ZIF-*gis*. Filled circles and open circles represent adsorption and desorption, respectively. **b** Sorption isotherm for H_2 (left) and D_2 (right) at various temperatures in Cu-ZIF-*gis*. Filled circles and open circles represent adsorption and desorption, respectively. **c** The contour map of the temperature-varied X-ray diffraction (XRD) pattern (left) of Cu-ZIF-*gis* over a temperature range from 20 K to 300 K. The structure of Cu-ZIF-*gis* exhibits temperature-dependent lattice expansion. At low temperatures, a rigid structure is formed. However, as the temperature increases, the lattice flexibility leads to a gating effect, allowing hydrogen isotope to enter the pores. The hydrogen isotherms are reproduced from ref.[31].

desorption below 60 K, indicating typical physical adsorption behavior (desorption energy ~ 5.61 kJ mol^{-1})[37]. However, MOF-74(Ni) with open metal sites as strong adsorption sites shows the desorption of hydrogen isotopes even above 90 K (heat of adsorption ~ 13 kJ mol^{-1})[8,38]. Partially fluorinated FMOF-Cu has three pores of different sizes, which are connected by a narrow bottleneck aperture[29]. This aperture allows H_2 access to the hidden third cavity through linker vibration. Due to this unique FMOF Cu structure, hydrogen isotopes could adsorb till 120 K. As another similar example, the metal-organic cage (MOC) material reported by He et al. consists of a flexible narrow window of 3.0 Å or less and organic macrocycles[30]. This material also exhibits a partial gate-opening effect, resulting in maximal desorption occurring at 100 K even in the absence of an open metal site. Still, a desorption signal starts to be observed at a very low temperature of 30 K, caused by interparticle spacing. Isostructural hexagonal metal-organic frameworks with 1-D channels (IFP-4) have a pore aperture of 1.7 Å[41]. While IFP-4 can adsorb hydrogen isotopes at high temperatures due to its thermally induced flexibility of very small apertures, the amount it can hold is quite limited, and desorption occurs similarly to MOC. Finally, it has been observed that in the Cu-ZIF-*gis*, hydrogen isotopes are desorbed completely at a temperature of 180 K, one of the highest compared to other materials reported previously. Releasing

https://doi.org/10.1038/s41467-025-56649-5

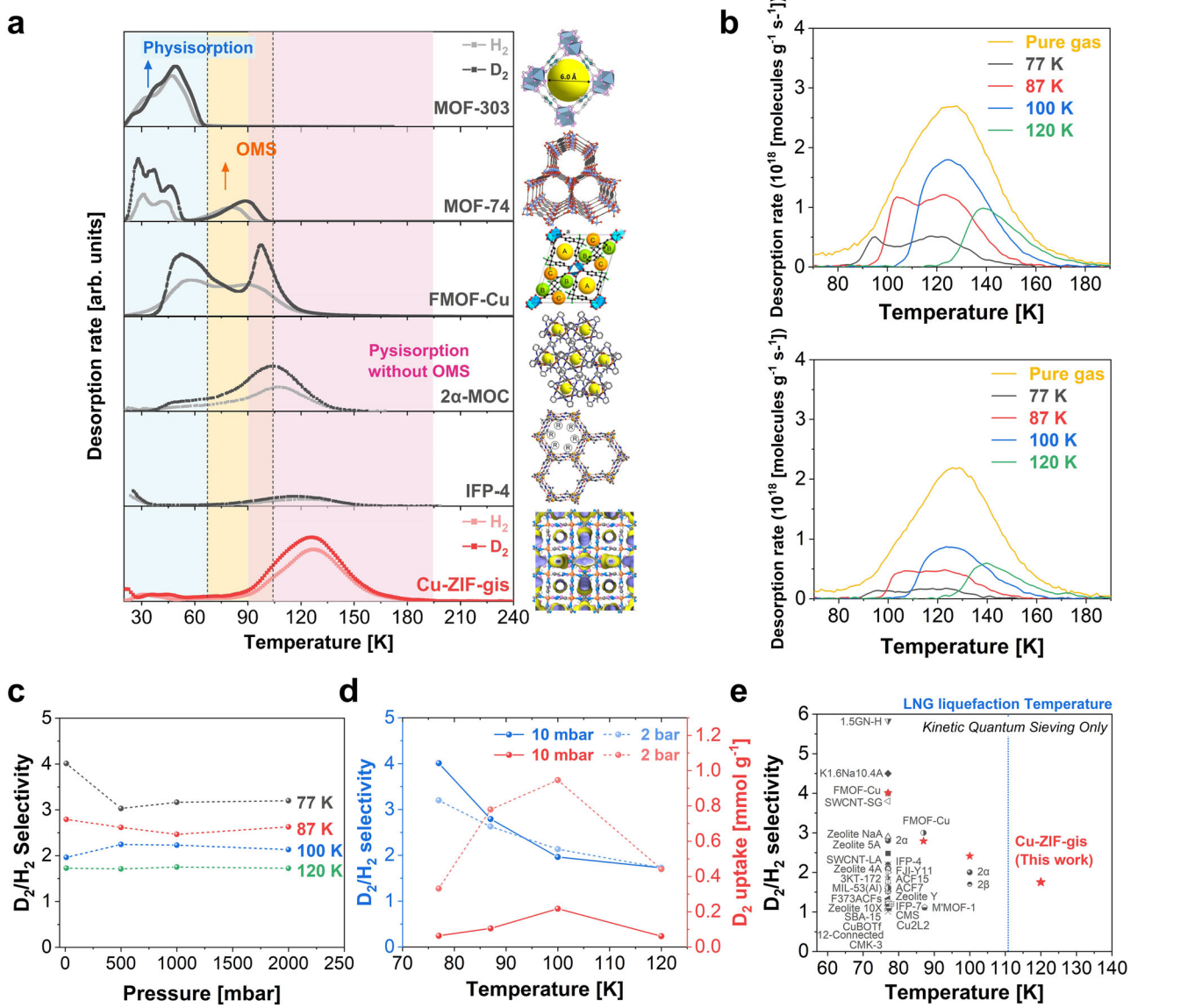

Fig. 3 | Thermal desorption spectroscopy (TDS) measurements of Cu-ZIF-*gis*. **a** TDS (Thermal desorption spectroscopy) spectra of Cu-ZIF-*gis* by exposing with Single-component H_2 and D_2 and comparison of its thermal desorption behavior with microporous MOF-303[37], MOF-74(Ni)[8] with open metal sites, partially fluorinated FMOF-Cu[29], IFP-4[41] and metal-organic cage (MOC) 2α[30] (**b**) D_2 (top) and H_2 (bottom) 1:1 mixture TDS spectra of a 2000 mbar on Cu-ZIF-*gis* at various temperature; 77 K (black), 87 K (red), 100 K (blue), 120 K (green). Each H_2 and D_2 in the mixture is plotted separately, and TDS spectra of pure H_2 and D_2 (yellow) are used to compare gas uptake. **c** The D_2/H_2 selectivity at various temperatures and loading pressures. **d** The D_2/H_2 selectivity corresponding to D_2 uptake at loading pressure of 10 and 2000 mbar in Cu-ZIF-*gis*. **e** The comparison of D_2/H_2 selectivity with various porous materials via kinetic quantum sieving (KQS) effect above 77 K.

the adsorbate at elevated temperatures emphasizes the diffusion limitations of hydrogen molecules through the 2.4 Å channels, even in the absence of strong adsorption sites.

Furthermore, desorption energy (E_d) was calculated using the Falconer and Madix equation, assuming that at peak temperature, the desorption peak maxima correspond to the desorption rate, and fractional surface coverage at desorption peak maxima is not a function of heating rate[39]. For E_d calculation, pure H_2 and D_2 TDS measured at 3, 4.5, and 6 K min^{-1} heating rates were used. Desorption energy is significantly influenced by adsorption enthalpy and the diffusion barrier within the narrow, one-dimensional channels. According to Panella et al., the adsorption enthalpy and desorption behavior are often interrelated, particularly in materials with small pore sizes due to increased potential overlap in micropores[40]. Typically, the diffusion barrier can be negligible in systems with larger pores. However, for porous materials with highly confined structures, such as Cu-ZIF-*gis*, the difference in diffusion barrier energy—resulting from enhanced van der Waals interactions in ultra-narrow nanopores—cannot be negligible and impacts the overall desorption energy. The E_d for H_2 and D_2 were almost identical values of 30.3 kJ mol^{-1} and 29.7 kJ mol^{-1}, respectively. Indeed, the surface binding energy (physisorption) of D_2 on Cu-ZIF-*gis* is typically higher than H_2 due to the quantum statistical mass effect[33], but the diffusion energy barrier difference by heating ramp rates of H_2 is higher than D_2 due to the *lattice-driven gating* effect in Cu-ZIF-*gis* during desorption (Supplementary Fig. 11).

The hydrogen isotope separation performance of Cu-ZIF-*gis* was investigated through TDS measurements for an equimolar H_2/D_2 mixture (Supplementary Fig. 9). TDS spectra and their selectivities ($S_{D2/H2}$) obtained at various exposure times (t_{exp} ~ 0.5, 60, and 120 min) at 1000 mbar (exposure pressure, P_{exp}) were shown in Supplementary Figs. 12, 13. Here, the exposure time and pressure refer to the gas environment to which the sample is exposed. The isotope uptake increased with exposure time but became mostly saturated after 60 min. These results imply almost equilibrium of isotope uptake at

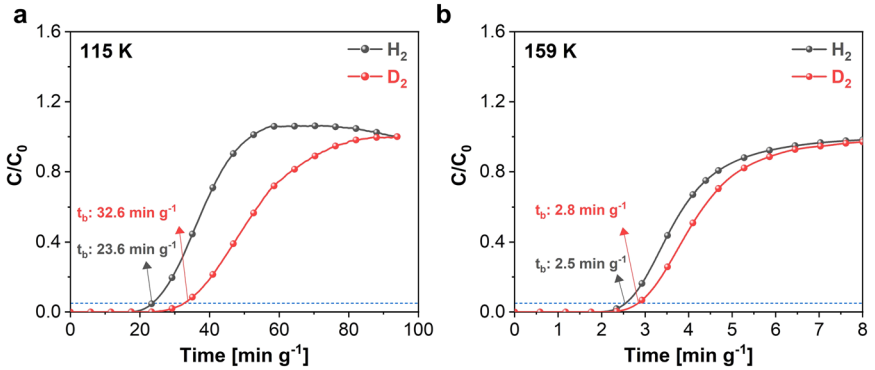

Fig. 4 | The breakthrough curve of H_2 and D_2 in Cu-ZIF-gis. a The breakthrough curve of H_2 (black) D_2 (red) was obtained by continuously flowing a Ne/H_2/D_2 (95.11/2.45/2.45 vol%) mixture with a total gas flow of 3.68 cc min^{-1} at 115 K. **b** The breakthrough curve was obtained at 159 K under same gas flow conditions. The blue dot line is breakthrough time, which corresponds to $C/C_0 = 0.05$.

60 min. Moreover, no significant change in $S_{D2/H2}$ was observed at all temperatures, even after 120 min exposure. Figure 3b and Supplementary Fig. 14 show TDS spectra of 1:1 H_2/D_2 mixture under different loading pressures (P_{exp} approximately up to 2000 mbar) and exposure temperatures (T_{exp} = 77–120 K) after 60 min of exposure (t_{exp}). Note that the TDS mixture spectra have been re-plotted separately for each isotope (Fig. 3b, top D_2, and bottom H_2). TDS analysis showed that the isotope uptake increased up to 100 K and revealed the existence of (at least) two major desorption peaks. As Cu-ZIF-*gis* has only one channel with no open metal site incorporated, the existence of two desorption peaks may imply two different desorbed phases caused by the thermal gating effect (Supplementary Fig. 15). Moreover, in the TDS spectrum, the desorption of D_2 was finished at around 140 K at T_{exp}~ 77 K, and completely desorbed at 180 K at T_{exp}~ 120 K. These results indicate that as the temperature increases, gas molecules can diffuse deeply into the internal channel, requiring higher temperatures to release internally trapped isotopes.

Figure 3c shows the D_2/H_2 selectivity ($S_{D2/H2}$) corresponding to the loading pressure (10–2000 mbar) and exposure temperature (77 – 120 K) at 60 min of exposure time. The $S_{D2/H2}$ at T_{exp}~ 77 K and P_{exp}~ 10 mbar was found to be 4.0. As the loading pressure increased, the $S_{D2/H2}$ decreased gradually and saturated to ca. 3.2 after 1000 mbar. At T_{exp}~ 87 K, the maximum $S_{D2/H2}$ of 2.8 was achieved at P_{exp}~ 10 mbar. With a further increase in the temperature, the $S_{D2/H2}$ decreases. The decrease in $S_{D2/H2}$ at higher temperatures can be ascribed to the progressive expansion of the lattice framework, resulting in getting larger channels and increased accessibility of both hydrogen isotopes. At 87, 100, and 120 K exposure temperatures, the $S_{D2/H2}$ remains constant or increases/decreases negligibly. The comparison of $S_{D2/H2}$ at 10 and 2000 mbar across various temperatures regarding the corresponding D_2 uptake is illustrated in Fig. 3d. It can be seen that the maximum $S_{D2/H2}$ of 4.0 at T_{exp}~ 77 K and 2000 mbar was obtained despite the lowest D_2 uptake. Based on the sorption isotherms, the LDG effect starts to be observed from 77 K, forming narrow pores for hydrogen isotopes in Cu-ZIF-*gis*. Therefore, the molecular confinement caused by the gating effect at 77 K maximizes, resulting in a high $S_{D2/H2}$ despite low isotope uptake. However, with increasing exposure temperature until 100 K, the signal intensity for both D_2 and H_2 increased, resulting in higher total isotope uptake, but due to the actively occurring gating effect caused by lattice expansion, accessibility of the pores to hydrogen isotopes is enhanced. As a result, the uptake of hydrogen isotope increased, leading to a decrease in $S_{D2/H2}$. Nevertheless, $S_{D2/H2}$ of 1.7 was still obtained even at a high temperature of 120 K and 2000 mbar, indicating that hydrogen isotope separation is possible at high temperatures and high pressures. It is worth noting that the exceptional performance of Cu-ZIF-*gis*, particularly in gas adsorption and diffusion, can be directly attributed to its inherent structural flexibility. While rigid frameworks with narrow 1D channels, such as IFP-4, are often hindered by diffusion limitations due to their lack of flexibility[41], Cu-ZIF-*gis* exhibits a distinct advantage through lattice expansion. This structural adaptability allows the framework to overcome the typical diffusion bottlenecks associated with narrow pore systems. Hence, highlighting the structural flexibility emphasizes its importance in the superior performance of Cu-ZIF-*gis*, especially when compared to less adaptable frameworks. These observations suggest that utilizing Cu-ZIF-*gis* can make the adsorptive D_2/H_2 separation process more energy efficient and benefit industrial processes requiring high pressure, such as the pressure swing adsorption (PSA) process.

As shown in Fig. 3e, the $S_{D2/H2}$ of Cu-ZIF-*gis* was compared with the previously reported $S_{D2/H2}$ of various MOFs exploiting the KQS effect (We intentionally excluded the CAQS materials due to their stability issues). Generally, the separation efficiency through KQS in most MOFs has been limited below 77 K, Supplementary Table 2. This is because, at high temperatures (above 77 K), hydrogen isotopes cannot attach to MOFs in an adsorbed state due to low binding energy. In the case of Cu-ZIF-*gis*, hydrogen isotopes are desorbed completely at a temperature of 180 K; therefore, the separation of D_2 and H_2 can be attempted at 120 K, which is one of the highest operating temperatures reported. As a result, Cu-ZIF-*gis* could be a promising adsorbent for increasing the operating temperature even above the LNG liquefaction temperature of 111 K of the KQS effect; the operating temperature of 111 K or higher means that LNG cryo-infrastructure already exists and can be used for isotope separation immediately.

To investigate the dynamic isotope separation performance of Cu-ZIF-*gis* for application in actual separation processes, dynamic isotope separation measurements were performed using a home-built breakthrough device[42]. Cu-ZIF-*gis* in pellet form was packed in the column, and a Ne/H_2/D_2 (95.11/2.45/2.45 vol%) mixture was continuously injected into the sample column at 115 K and 159 K at a total gas flow of 3.68 cc min^{-1}. (Fig. 4a, b) At 115 K, a signal of H_2 is observed at 23.6 min g^{-1}, whereas D_2 is maintained at 32.6 min g^{-1}. D_2 has a longer breakthrough time than H_2, which means that D_2 is preferentially adsorbed in Cu-ZIF-*gis*. The breakthrough time difference between H_2 and D_2 decreased with increasing temperature, but D_2 was maintained for 2.8 min g^{-1} at 159 K. The hydrogen isotope dynamic separation performance of Cu-ZIF was calculated as shown in Supplementary Fig. 16. The D_2/H_2 selectivity was 1.5 and 1.3 at 115 K and 159 K, respectively. Thus, using dynamic isotope separation measurements, Cu-ZIF-gis can be used for hydrogen isotope separation even at high temperatures.

Microscopic observation of diffusion dynamics

Quasi-elastic neutron scattering (QENS) analysis further elucidates the role of thermal lattice expansion in Cu-ZIF-*gis* for hydrogen isotope separation, providing deeper insights into H_2 and D_2 motion in Cu-ZIF-

https://doi.org/10.1038/s41467-025-56649-5

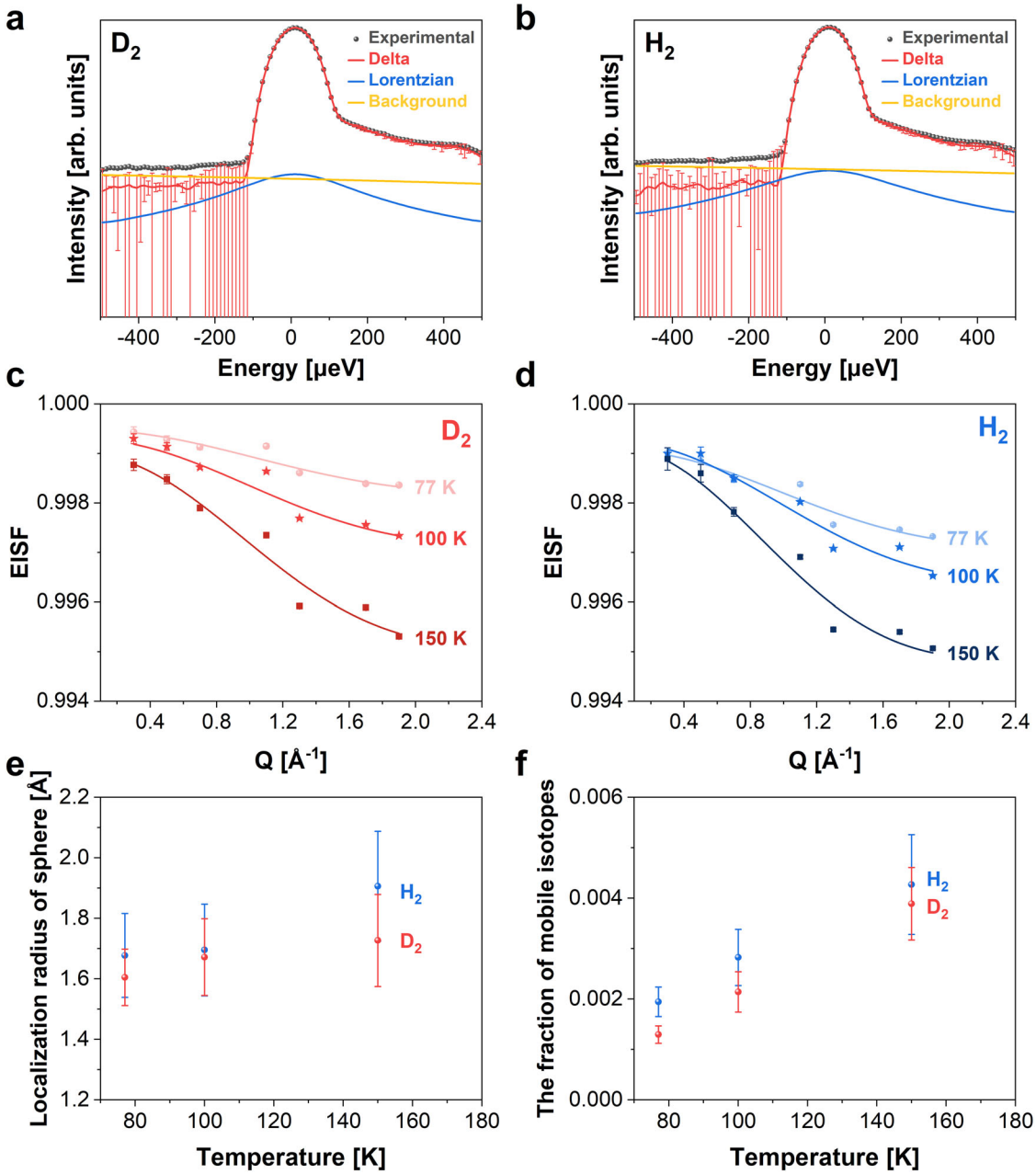

Fig. 5 | Quasi-elastic neutron scattering (QENS) experiments and the Elastic incoherent structure factor (EISF) fitting. a Quasi-elastic neutron scattering (QENS) spectrum for D_2 at 77 K and 0.7 mmol g^{-1} of pressure loading in Cu-ZIF-*gis* (black circles: raw data, red line: delta function, blue line: Lorentzian and yellow line: background). **b** QENS spectrum for H_2 at 77 K and 0.7 mmol g^{-1} of pressure loading in Cu-ZIF-*gis* (black circles: raw data, red line: delta function, blue line: Lorentzian and yellow line: background). The errors in (**a**, **b**) correspond to estimates of the standard deviation of the parameter, assuming the parameters follow a Gaussian distribution. Also, note that the vertical scale in this figure is logarithmic. **c** The EISF of 0.7 mmol g^{-1} D_2 at 77 K (circles), 100 K (stars), and 150 K (squares) as a function of momentum transfer. The solid lines represent the fitting data of Elastic incoherent structure factor (EISF) obtained using the diffusion in a sphere model proposed by Volino and Dianoux[48]. **d** The EISF of 0.7 mmol g^{-1} H_2 at 77 K (circles), 100 K (stars), and 150 K (squares) as a function of momentum transfer. The solid lines represent the fitting data of EISF obtained using the diffusion in a sphere model proposed by Volino and Dianoux[48]. **e** The radius of a sphere for H_2 (blue) and D_2 (red) in Cu-ZIF-*gis*, was obtained from the EISF fitting parameter. **f** The fraction of mobile H_2 (blue) and D_2 (red) in the confined pore of Cu-ZIF-gis, was obtained from the EISF fitting parameter. The error bars in the (**e**, **f**) indicate standard deviation.

gis[43–45]. Our QENS analysis reveals the temperature-dependent mobility of adsorbed hydrogen isotopes within the Cu-ZIF-*gis* framework. The fitting process for QENS data was performed using the QCLIMAX package in the Integrated Computational Environment-Modeling & Analysis for Neutrons(ICE-MAN)[46]. Despite the experimental data's asymmetry (originating from the instrument), the obtained QENS spectra are well-fitted with delta, Lorentzian functions, and constant background (Fig. 5a, b and Supplementary Figs. 17–32). The delta Function (red line) represents the elastic scattering component, indicating the presence of immobile or very slow-moving isotopes within the pores of Cu-ZIF-*gis*. The broad Lorentzian (blue line) component accounts for the quasi-elastic scattering, indicating the isotope molecule's diffusive motion. The width of the Lorentzian peak provides information about the diffusion coefficients and the nature of the molecular motion. Constant background (yellow line) accounts for any residual background noise of the measured data. We have analyzed the

Table 1 | Fraction of mobile molecules and localization radius at various temperatures in Cu-ZIF-*gis* determined by hydrogen isotope diffusion model Eq. (2)

Temperature [k]	Mobile Fraction [%]		Localization of radius, *r* [Å]	
	H_2	D_2	H_2	D_2
77	0.20 ± 0.03	0.13 ± 0.02	1.68 ± 0.14	1.61 ± 0.09
100	0.28 ± 0.06	0.21 ± 0.04	1.70 ± 0.15	1.67 ± 0.13
150	0.43 ± 0.10	0.39 ± 0.07	1.91 ± 0.18	1.73 ± 0.15

* Please note that the immobile fraction also contains the Cu-ZIF-*gis* itself.

Elastic Incoherent Structure factor (EISF), which is the contribution of elastic scattering to the total scattering intensity (elastic+quasielastic) and provides details about localized hydrogen isotope motion geometry[47]. (Eq. (1))

$$EISF(Q) = \frac{I_{elastic}(Q)}{I_{elastic}(Q) + I_{Quasielastic}(Q)} \quad (1)$$

The geometry of the confined molecular motion of hydrogen isotopes can be determined by fitting the Q-dependence of the EISF. Therefore, the diffusion in a sphere model derived by Volino and Dianoux has been employed to describe the localized motions of isotopes within the confined space[48].

$$EISF(Q) = A + (1 - A)\left(\frac{3j_1(Qr)}{Qr}\right)^2 \quad (2)$$

Where A is the fraction of immobile molecules, while (1-A) is the fraction of mobile molecules that undergo localized motions within a sphere of radius r, and j_1 is the spherical Bessel function of the first order. As shown in Fig. 5c, d, the fitting of the EISF for H_2 and D_2 at various temperatures were obtained using Eq. 2. The diffusion in a sphere model analysis shows a greater confinement effect for D_2 compared to H_2 within the Cu-ZIF-*gis* structure, suggesting differential mobility that facilitates effective isotope separation. This is particularly evident at low loading (0.7 mmol g^{-1}), where the localization radius for H_2 (1.7–1.9 Å) was also larger than that for D_2 (1.6–1.7 Å) (Fig. 5e and Table 1) across all exposure temperatures, indicating that H_2 undergoes diffusive motion within these confined pores, whereas D_2 appears to be more confined and immobilized (see mobile fraction of (1-A), Fig. 5f and Table 1). This means D_2 is more likely to remain within the porous framework than H_2, which also aligns with previously reported results[49]. Hence, this subtle difference in single-component isotopes of r and A values in Fig. 5e, f implies that the temperature-dependent mobility of D_2 is more pronounced than H_2, potentially affecting separation selectivity under the mixture.

Our study concludes by demonstrating the mechanism of *lattice-driven gating* and highlighting the exceptional performance and robustness of Cu-ZIF-*gis*, a Cu-based ZIF, for hydrogen isotope separation. We mainly focused on its efficiency at elevated temperatures and pressures. Our advanced cryogenic TDS measurements reveal that Cu-ZIF-*gis* maintains significant D_2/H_2 selectivity even above the LNG temperature of 111 K. This performance based on the KQS is significantly higher than the operational temperatures for traditional methods (or any other KQS materials), attributed to the material's *lattice-driven gating* effect, which dynamically modulates pore sizes to optimize isotope separation. The temperature-triggered lattice-driven gating in Cu-ZIF-*gis* enhances its ability to adsorb and separate hydrogen isotopes at elevated temperatures at 120 K, allowing for efficient separation of D_2 from H_2 under high-pressure conditions, thereby eliminating the need for low-temperature operations. Interestingly, its operating temperature above 111 K makes it a viable solution for integration into existing LNG cryo-infrastructure, facilitating large-scale industrial applications. The material also exhibits excellent structural stability, retaining its framework integrity even after prolonged (for 38 months) exposure to air and multiple adsorption-desorption cycles, ensuring long-term performance and reliability in industrial settings. Complementary QENS experiments support the findings. These experiments reveal a dynamic difference that allows for the effective separation of D_2 from H_2, even at temperatures up to 150 K. This highlights that Cu-ZIF-*gis* offers a breakthrough strategy for hydrogen isotope separation. It leverages both the *lattice-driven gating* effect and the distinct mobility dynamics revealed by QENS to achieve high performance under practical conditions. The Cu-ZIF-*gis* demonstrates high efficiency at elevated temperatures and pressures, alongside robust durability, overcoming the limitations of conventional methods while providing a more energy-efficient and environmentally sustainable alternative.

Methods

Material synthesis

Cu-ZIF-*gis* was prepared on a 5-fold scale using the literature method[31]. $Cu(NO_3)_2{\cdot}3H_2O$ (121 mg, 0.5 mmol, Sigma-Aldrich) and 2-nitroimidazole (113 mg, 1.0 mmol, TCI) were dissolved in *N,N*-dimethylformamide (DMF) (15 mL, Daejung Chemicals & Metals Co., Ltd.) in a 30 mL vial. The vial was tightly capped with Teflon tape and heated in an oven at 80 °C for one day to give blue square crystals. The crystals were filtered and washed with neat DMF (10 mL × 3) and diethyl ether (10 mL × 3) and dried under reduced pressure for about ten hours. The yield was 40% based on one mole of the metal salt[31].

General materials characterization

X-ray diffraction (XRD) experiment was carried out on the Rigaku MiniFlex 600 using Cu Kα radiation in the 2θ range of 5°–40° with a scanning rate of 10 deg min^{-1}. Fourier transform infrared (FT-IR) was obtained under transmission mode in the range of 4000–500 cm^{-1} using Thermo Fisher Scientific Nicolet iS50. Thermogravimetric analysis (TGA) was conducted in a temperature range from 25 °C to 700 °C with a heating rate of 10 °C min^{-1} under N_2 atmosphere with a flow rate of 15 cc min^{-1} using TGA-N-1000.

Gas sorption isotherms measurement

A H_2, D_2, and O_2 sorption experiment was conducted by a fully automated Quantachrome Autosorb-iQ2 with a home-built temperature-controlled cryocooler. Temperature calibration was performed due to the difference in position between the temperature sensor and the sample. The exact temperature was determined through the saturation pressure of various gases (H_2, D_2, O_2). In addition, volume calibration was performed using the exact temperature obtained through temperature calibration. The existing volume calibration method using helium has a problem with helium adsorption at cryogenic temperatures. Therefore, the adsorption amount of the empty cell at each temperature was measured using a measuring gas, and then the measured value of the sample cell containing the sample was calibrated. Prior to measurement, Cu-ZIF-*gis* (ca. 100 mg) was activated under an ultra-high vacuum at 433 K for 10 h to remove the moisture and gas molecules. The H_2 and D_2 sorption isotherms were obtained at 40, 77, 87, 100, 120, and 150 K, and O_2 sorption isotherms were obtained at 90, 110, 135, 160, 185, and 210 K.

Temperature-varied X-ray diffraction patterns (XRD) measurement

Temperature-varied XRD measurements were conducted to investigate the structural transition in Cu-ZIF-*gis* as a function of temperature. Structural studies of the Cu-ZIF-*gis* were performed using Rigaku MiniFlex 600 with CuKα radiation. Prior to measurement, Cu-ZIF-*gis*

was activated at 100 °C for 3 h to remove the moisture and impurities. Temperature-varied XRD pattern was recorded within the 14°–20° range with a scanning speed of 3 deg min^{-1} in a temperature range of 20 K–300 K with a heating rate of 6 K min^{-1} under vacuum conditions.

Thermal desorption spectroscopy (TDS) measurement

TDS experiment was performed using an advanced cryogenic thermal adsorption spectroscopy (AC-TDS) apparatus equipped with quadrupole mass spectroscopy (QMS) and turbo molecular pump (TMP) for ultrahigh vacuum (10^{-8} mbar). The sample was loaded in a Copper sample holder and activated under vacuum at 433 K for 5 hours in order to remove water and adsorbed gas impurities if any. The procedure of TDS measurement proceeded as shown in Supplementary Fig. 9. For pure H_2 and D_2 TDS measurement, the sample was exposed to pure H_2 or D_2 at room temperature and liquefaction temperature (20 K for H_2, 23 K for D_2). Afterward, unadsorbed gas was evacuated at 20/23 K and cooled down to 18 K, and finally, the sample was heated to 240 K with a ramping rate of 6 K min^{-1}. The desorbing gas was continuously recorded by quadrupole mass spectroscopy (QMS). In the H_2/D_2 1:1 mixture measurements, the sample was exposed to H_2/D_2 1:1 mixture at various exposure temperatures (77, 87, 100, and 120 K) for 60 min, and unadsorbed gas was evacuated at exposure temperatures. Then, the sample was cooled down to 18 K. Subsequently, with an increase in the temperature with a ramping rate of 6 K min^{-1} to 240 K, the gas molecules started desorbing from the sample and were quantified by QMS. The area under the obtained desorption peak of H_2 and D_2 was proportional to the desorbed amount of hydrogen isotopes, which can be quantified after calibration of TDS. The $S_{D2/H2}$ was directly calculated using the quantified area under desorption peak by calibration constant after calibration of TDS using $Pd_{95}Ce_5$ alloy and TiH_2 powder.

Dynamic hydrogen isotope separation measurement

Dynamic hydrogen isotope separation was measured using a home-built breakthrough device equipped with quadrupole mass spectrometer (QMS) QGA from Hiden Analytical[42]. A 1.832 g sample was loaded into a stainless-steel sample column with a height of 120.0 mm and an inner diameter of 4.2 mm. It was then activated under vacuum at 433 K for 8 h to remove water and adsorbed gas impurities. The procedure of breakthrough measurement was done as follows: The gas composition of the inlet feed was controlled precisely by using a mass flow controller (MFC) under 0.01 sccm resolution. Neon was filled in both, the bypass and the sample column until 1000 mbar of pressure, and then flow was guided to the bypass column with an additional flow of He under a constant flow rate of 0.18 sccm. Once the composition was stabilized, the feed gas was guided to the sample column for void volume correction. Then, the helium flow was stopped, and neon was flushed until the residue of helium in the sample column disappeared. Then, the feed gas was guided back to the bypass line with an additional flow of H_2 and D_2 under a constant flow rate of 0.09 sccm for each component with a flow rate ratio of 1:1. Once QMS detected the stable composition of the outlet feed, the feed direction was guided to the sample column to conduct dynamic hydrogen isotope separation. Depending on the affinity, the gas with higher uptake showed a longer retention time, indicating more uptake. For cryogenic measurements of 115 K and 159 K, refrigerant using a mixture of liquid nitrogen (LN_2) and isopentane for 115 K and ethanol for 159 K was used. Also, to minimize the heat provided by feed gas, a pre-cooling site filled with LN_2 was applied before the sample column during cryogenic measurements. The obtained signal intensity was normalized with the equilibrium intensity of each gas and the area's integral until the equilibrium point was measured and subtracted from the inlet feed to measure the uptake and calculate selectivity $S_{D2/H2}$.

Quasi-elastic neutron scattering (QENS) Measurements

The QENS measurement was carried out by disk chopper time-of-flight (TOF) spectrometer, IN5 at the Institut Laue-Langevin (Grenoble, France). The QENS spectra were collected using an incident neutron with a wavelength of 5 Å in a momentum transfer range of 0.3 $Å^{-1}$ to 1.9 $Å^{-1}$ with a step size of 0.2 $Å^{-1}$. The sample was loaded into an aluminum sample can in the glove box to prevent air exposure. Before the QENS measurement, the sample holder loaded Cu-ZIF-*gis* was activated at 433 K under a vacuum condition to remove the moisture and impurities. Afterward, the sample can be transferred to the IN5. During QENS measurement, H_2, and D_2 gases were injected into the sample, dosing amounts of 0.7 and 2.0 mmol g^{-1} at each temperature (77 K–150 K) through an in situ gas dosing system. The standard vanadium and empty can measurements were conducted for data normalization and background correction.

Data availability

All data involved in this work are included in this article and the corresponding Supplementary Information. Source data are provided in this paper.

References

1. Avouris, P. et al. STM-induced H atom desorption from Si (100): isotope effects and site selectivity. *Chem. Phys. Lett.* **257**, 148–154 (1996).
2. Cheng, K., Lee, J. & Lyding, J. W. Approach to enhance deuterium incorporation for improved hot carrier reliability in metal-oxide-semiconductor devices. *Appl. Phys. Lett.* **77**, 2358–2360 (2000).
3. Lyding, J. W., Hess, K. & Kizilyalli, I. C. Reduction of hot electron degradation in metal oxide semiconductor transistors by deuterium processing. *Appl. Phys. Lett.* **68**, 2526–2528 (1996).
4. Greenwood, N. N. & Earnshaw, A. *Chemistry of the Elements*. (Elsevier, 2012).
5. Oak Ridge National Laboratory. Materials for Separation Technologies: Energy and Emission Reduction Opportunities. (2005)
6. Bondorf, L. et al. Isotope-selective pore opening in a flexible metal-organic framework. *Sci. Adv.* **8**, eabn7035 (2022).
7. Savchenko, I. et al. Hydrogen isotope separation in metal-organic frameworks: Kinetic or chemical affinity quantum-sieving? *Microporous Mesoporous Mater.* **216**, 133–137 (2015).
8. Kim, J. Y. et al. Exploiting diffusion barrier and chemical affinity of metal–organic frameworks for efficient hydrogen isotope separation. *J. Am. Chem. Soc.* **139**, 15135–15141 (2017).
9. Muhammad, R. et al. Exploiting the specific isotope-selective adsorption of metal–organic framework for hydrogen isotope separation. *J. Am. Chem. Soc.* **143**, 8232–8236 (2021).
10. Park, J., Attia, N. F., Jung, M., Lee, K. & Oh, H. Biobased derived nanoporous carbon for hydrogen isotope separation. *Microporous Mesoporous Mater.* **304**, 109291 (2020).
11. Xiong, R. et al. Hydrogen isotopes separation in Ag (I) exchanged ZSM-5 zeolite through strong chemical affinity quantum sieving. *Microporous Mesoporous Mater.* **313**, 110820 (2021).
12. Kim, J. Y., Oh, H. & Moon, H. R. Hydrogen isotope separation in confined nanospaces: Carbons, zeolites, metal–organic frameworks, and covalent organic frameworks. *Adv. Mater.* **31**, 1805293 (2019).
13. Ha, J., Jung, M., Park, J., Oh, H. & Moon, H. R. Thermodynamic separation of hydrogen isotopes using hofmann-type metal–organic frameworks with high-density open metal sites. *ACS Appl. Mater. Interfaces* **14**, 30946–30951 (2022).
14. Oh, H. et al. A cryogenically flexible covalent organic framework for efficient hydrogen isotope separation by quantum sieving. *Angew. Chem. Int. Ed.* **52**, 13219–13222 (2013).

15. Weinrauch, I. et al. Capture of heavy hydrogen isotopes in a metal-organic framework with active Cu (I) sites. *Nat. Commun.* **8**, 14496 (2017).
16. Zhang, L. et al. Chemical affinity of Ag-exchanged zeolites for efficient hydrogen isotope separation. *Inorg. Chem.* **61**, 9413–9420 (2022).
17. Oh, H., Savchenko, I., Mavrandonakis, A., Heine, T. & Hirscher, M. Highly effective hydrogen isotope separation in nanoporous metal–organic frameworks with open metal sites: direct measurement and theoretical analysis. *ACS Nano* **8**, 761–770 (2014).
18. Xiong, R. et al. Highly effective hydrogen isotope separation through dihydrogen bond on Cu (I)-exchanged zeolites well above liquid nitrogen temperature. *Chem. Eng. J.* **391**, 123485 (2020).
19. Katugampalage, T. R. et al. Bimetallic Fe: Co metal–organic framework (MOF) with unsaturated metal sites for efficient Fenton-like catalytic degradation of oxytetracycline (OTC) antibiotics. *Chem. Eng. J.* **479**, 147592 (2024).
20. Kim, J. Y. et al. Selective hydrogen isotope separation via breathing transition in MIL-53 (Al). *J. Am. Chem. Soc.* **139**, 17743–17746 (2017).
21. Teufel, J. S. Experimental investigation of H2/D2 isotope separation by cryo-adsorption in metal-organic frameworks. (2012).
22. Aljammal, N., Jabbour, C., Chaemchuen, S., Juzsakova, T. & Verpoort, F. Flexibility in metal–organic frameworks: A basic understanding. *Catalysts* **9**, 512 (2019).
23. Chen, K. et al. Gating effect for gas adsorption in microporous materials—mechanisms and applications. *Chem. Soc. Rev.* **51**, 1139–1166 (2022).
24. Schneemann, A. et al. Flexible metal–organic frameworks. *Chem. Soc. Rev.* **43**, 6062–6096 (2014).
25. Kotani, R., Kondo, A. & Maeda, K. Gate adsorption of CO 2 on a flexible one-dimensional copper-based coordination polymer crystal. *ChemComm* **48**, 11316–11318 (2012).
26. Zhao, D., Yuan, D., Krishna, R., van Baten, J. M. & Zhou, H.-C. Thermosensitive gating effect and selective gas adsorption in a porous coordination nanocage. *ChemComm* **46**, 7352–7354 (2010).
27. Ma, S., Sun, D., Wang, X. S. & Zhou, H. C. A mesh-adjustable molecular sieve for general use in gas separation. *Angew. Chem. Int. Ed.* **46**, 2458–2462 (2007).
28. Kim, H. et al. Temperature-triggered gate opening for gas adsorption in microporous manganese formate. *ChemComm* **39**, 4697–4699 (2008).
29. Zhang, L. et al. Exploiting dynamic opening of apertures in a partially fluorinated MOF for enhancing H2 desorption temperature and isotope separation. *J. Am. Chem. Soc.* **141**, 19850–19858 (2019).
30. He, D. et al. Hydrogen isotope separation using a metal–organic cage built from macrocycles. *Angew. Chem. Int. Ed.* **61**, e202202450 (2022).
31. Jung, C. et al. Porous zeolitic imidazolate frameworks assembled with highly-flattened tetrahedral copper (ii) centres and 2-nitroimidazolates. *ChemComm* **59**, 4040–4043 (2023).
32. Nam, J. et al. Zeolitic imidazolate frameworks as solid-state nanomachines. *Angew. Chem. Int. Ed.* **63**, e202404061 (2023).
33. Chen, B. et al. Surface interactions and quantum kinetic molecular sieving for H_2 and D_2 adsorption on a mixed metal– organic framework material. *J. Am. Chem. Soc.* **130**, 6411–6423 (2008).
34. Javed, A., Strauss, I., Bunzen, H., Caro, J. & Tiemann, M. Humidity-mediated anisotropic proton conductivity through the 1D channels of Co-MOF-74. *Nanomaterials* **10**, 1263 (2020).
35. Li, J.-N. et al. Host–Host interactions enhanced the structural rigidity in a 6-Fold interpenetrated diamondoid metal–organic framework exhibiting C_2H_2/C_2H_4 separation. *Inorg. Chem.* **63**, 8286–8293 (2024).
36. Miyazaki, I., Masuoka, Y., Suzumura, A., Moribe, S. & Umehara, M. Direct sintering behavior of metal organic frameworks/coordination polymers. *ACS Omega* **7**, 47906–47911 (2022).
37. Kim, H. et al. High D_2/H_2 selectivity performance in MOF-303 under ambient pressure for potential industrial applications. *Sep. Purif. Technol.* **325**, 124660 (2023).
38. Pham, T. et al. Understanding the H_2 sorption trends in the M-MOF-74 series (M= Mg, Ni, Co, Zn). *J. Phys. Chem. C* **119**, 1078–1090 (2015).
39. Falconer, J. L. & Schwarz, J. A. Temperature-programmed desorption and reaction: applications to supported catalysts. *Catal. Rev. Sci. Eng.* **25**, 141–227 (1983).
40. Panella, B. et al. Desorption studies of hydrogen in metal–organic frameworks. *Angew. Chem. Int. Ed.* **47**, 2138–2142 (2008).
41. Mondal, S. S. et al. Systematic experimental study on quantum sieving of hydrogen isotopes in metal-amide-imidazolate frameworks with narrow 1-D channels. *Chem. Phys. Chem* **20**, 1311–1315 (2019).
42. Jung, S.-Y., Park, D., Kim, S. & Oh, H. Comprehensive design and experimental protocol for scalable and temperature-controllable cryogenic hydrogen isotope separation. *Anal. Chem.* **96**, 20277–20286 (2024).
43. NaraseGowda, S., Brown, C. M., Tyagi, M., Jenkins, T. & Dobbins, T. A. Quasi-elastic neutron scattering studies of hydrogen dynamics for nanoconfined NaAlH4. *J. Phys. Chem. C* **120**, 14863–14873 (2016).
44. Jung, M. et al. Elucidation of diffusivity of hydrogen isotopes in flexible MOFs by quasi-lastic neutron scattering. *Adv. Mater.* **33**, 2007412 (2021).
45. Pefoute, E., Kemner, E., Soetens, J., Russina, M. & Desmedt, A. Diffusive motions of molecular hydrogen confined in THF clathrate hydrate. *J. Phys. Chem. C* **116**, 16823–16829 (2012).
46. Ramirez-Cuesta, A. J. & Cheng, Y. The ICEMAN, a heterogeneous platform for analysis of neutron scattering data. *Neutron News* **32**, 15–16 (2021).
47. Bée, M. A physical insight into the elastic incoherent structure factor. *Physica B Condens. Matter* **182**, 323–336 (1992).
48. Volino, F. & Dianoux, A. Neutron incoherent scattering law for diffusion in a potential of spherical symmetry: general formalism and application to diffusion inside a sphere. *Mol. Phys.* **41**, 271–279 (1980).
49. Yang, D. et al. Investigation of the dynamic behaviour of H_2 and D_2 in a kinetic quantum sieving system. *ACS Appl. Mater. Interfaces* **16**, 12467–12478 (2024).

Acknowledgements

This research was funded by the National Research Foundation of Korea (NRF), Government of Korea (MSI) (2022R1A2C3005978, RS-2023-00281671, NRF-2020R1A2C1004717). The computing resources were made available through the VirtuES and the ICE-MAN projects, funded by the Laboratory Directed Research and Development program and Compute and Data Environment for Science (CADES) at ORNL. We acknowledge the Institut Laue-Langevin (Grenoble, France) for the allocation of beam time.

Author contributions

M.J., J.P., and H.O. conceptualized the project. M.J., J.P., and R.M. developed the methodology. C.J. and J.K. synthesized and characterized the sample. M.J., J.P., and T.P. performed sorption & TDS experiments and analyzed the data. J.Y. conducted temperature-varied XRD measurement. S.J. conducted dynamic breakthrough measurements. M.J., J.P., J.O., J.T.P., and M.R. performed the QENS experiment, and M.J., J.P., A.J.R.-C., J.T.P., M.R., and H.O. analyzed and visualized the data. H.O. was responsible for funding acquisition and provided supervision throughout the project. M.J., J.P., R.M., J.K., M.R., and H.O. wrote the original draft. M.J., J.P., R.M., J.T.P., J.K., M.R., and H.O. reviewed and edited the paper.

Competing interests

The authors declare no competing interests.

Additional information

Supplementary information The online version contains supplementary material available at https://doi.org/10.1038/s41467-025-56649-5.

Correspondence and requests for materials should be addressed to Jaheon Kim, Margarita Russina or Hyunchul Oh.

Peer review information *Nature Communications* thanks Hoi Ri Moon and the other anonymous reviewer(s) for their contribution to the peer review of this work. A peer review file is available.